Feasibility Study of Optical Space Situational Awareness from Sun-Earth L1

Erik D. Payton
University of Maryland
Tam Nguyen
University of Maryland

ABSTRACT

Recent interests in lunar missions and cislunar operations motivate the need for space situational awareness (SSA) capabilities for resident space objects (RSOs) in cislunar space. The space surveillance network (SSN), which primarily consists of Earth-based sensors, is the current standard for SSA. However, cislunar SSA from ground-based sensors is challenging due to sensor gaps and poor viewing angles, even while utilizing a global network. The first Sun-Earth Lagrange point (SEL1), not usually considered for cislunar SSA as target RSOs viewed from such an extreme distance have very low signal-to-noise ratios (SNR), has geometric, photometric, and astrodynamics advantages that are hard to achieve in other orbital regimes. The sensitivity gap can be mitigated by methods such as track-before-detect (TBD), which detect faint objects by adding low SNR signals in successive frames to make un-cued detections on a blind search. This work presents an overview mission concept for a SEL1 cislunar observer, focusing on the preliminary design of the optical system and operational procedures. The scope includes trade studies over the design architectures for the optical tube assemblies (OTAs), as well as operational approaches that can be employed to maximize the single-frame SNR before starting a blind search. One such proposed method uses multiple co-boresighted OTAs and synthetic tracking along known motion vectors to increase SNRs in the images before un-cued detections are made. Preliminary results show that an example design for an observatory with four co-boresighted 30 cm f/1.4 OTAs has the potential to detect meter-sized objects in cislunar space with a 50% probability of detection and 1% false alarm rate. This work serves as a baseline for future system and mission design studies for SEL1 cislunar SSA concepts.

1. INTRODUCTION

Current space situational awareness (SSA) architectures are primarily focused on detection and tracking of Earth-orbiting spacecraft and debris. With recent interest in lunar missions and cislunar operations, SSA capabilities for resident space objects (RSOs) in cislunar space must be developed. Current SSA efforts rely on the space surveillance network (SSN), which primarily consists of ground-based sensors [2]. It has been shown that cislunar SSA from ground-based sensors is challenging due to coverage gaps and poor viewing angles, even while utilizing a global network of sensors. These systems are also subject to operational constraints imposed by the viewing conditions required for optical observations, including darkness and weather [6, 9]. Space-based SSA sensors have the potential to address the cislunar SSA problem. Earth-orbiting sensors offer a potential solution but retain several limitations of ground-based systems, while introducing additional constraints on size and power. Their space-based vantage point eliminates atmospheric light scattering and enables near-continuous observations, subject primarily to exclusion zones around the Earth, Sun, and Moon [5, 9]. A sensor placed in a cislunar orbit would avoid some of the challenges with Earth-orbiting spacecraft; however, complex orbital dynamics in the cislunar regime result in few orbits that provide consistent favorable solar illumination angles, long-term stability, and extensive optical coverage of the regime [6, 22].

The first Sun-Earth Lagrange point (SEL1), located 1.5 million kilometers from the Earth-Moon system, is not often considered for SSA. Detection of a spacecraft from these extreme distances is challenging due to significant flux losses. Despite this challenge, SSA from SEL1 provides optical advantages otherwise unachievable, offering a near-zero phase angle and a comprehensive view of the Earth-Moon system with limited exclusion zones. Additionally, SEL1 orbits have long-term stability with minimal delta-v cost for orbit maintenance [17].

This paper investigates the feasibility of placing a SSA spacecraft at the SEL1 point, considering several optical designs with various hardware and operational constraints. A brief overview is given of the relevant optics concepts, as well as an introduction to faint-object detection methods. The concept of operations is introduced to outline the parameters of the trade study, and then results are shown with and without losses due to image processing methods. An example design is provided as a feasible solution to mmotivatefuture work in optimizing this architecture.

Copyright © 2026 Advanced Maui Optical and Space Surveillance Technologies Conference (AMOS) – www.amostech.com

2. BACKGROUND

2.1 Challenges of Cislunar SSA

Comprehensive cislunar SSA is a challenging problem for several reasons. The search volume for cislunar space is much larger than for geostationary orbits (GEO) and below. More conservative estimates of the volume place the total space at over 1700 times larger than that within the GEO belt [9]. Extreme distances between the Earth and Moon present increased problem complexity as a complete search takes longer, and target RSOs beyond GEO orbits appear much fainter. For example, an object in a lunar orbit is approximately ten times the distance of a GEO orbit as observed from a ground sensor, which translates to a one hundred times reduction in observed brightness. Already faint signals are further degraded near the brightly illuminated lunar surface, adding additional background noise and further decreasing the signal-to-noise ratio (SNR) of the RSO. In addition to the optical challenges associated with cislunar SSA, there are also difficulties due to limited infrastructure. Relying on the SSN for cislunar SSA imposes significant challenges. Sensors gaps and poor viewing angles lead to faint and unreliable detections, compounding the operational difficulty of making detections of spacecraft in dynamically complex orbits with architectures designed for simple two-body motion [6, 18].

Architectures to complement the SSN exist both in development and in literature. The most popular option for near-Earth SSA is by far ground-based sensors. These sensors can be optical or other options such as passive RF [9, 11]. While the most plentiful and easy to build, these sensors have severe limitations in terms of object tracking, as a continuous track will almost never be achievable with one sensor. In the space-based regime, the Oracle Family of Systems in development with the Air Force Research Laboratory (AFRL) presents an alternative solution, placing a cislunar SSA satellite in an orbit between the Earth and Moon [12]. Work by Vendl and Holzinger [22] shows that retrograde periodic orbits with m:n periods resonant with the Moon's synodic period possess strong characteristics for cislunar SSA. They find that certain L1 and L2 Lyapunov trajectories are near optimal for phasing with illuminated regions of interest; however, this does not mitigate all the challenges. Another alternative is centered around lunar surface hardware using COTS sensors on the lunar surface to assist with SSA efforts [24]. This avoids some difficulties associated with space-based sensors, but this concept faces similar coverage limitations as those on Earth.

While cislunar sensors benefit from shorter detection distances, SEL1 offers long-term orbital stability with minimal ΔV requirements [15, 16, 17]. However, detections from SEL1 require observing across a distance of approximately 1.5 million km, causing GEO RSOs to appear roughly 1600 times fainter at SEL1 than they would if observed from the Earth's surface. A spacecraft positioned at SEL1 for cislunar SSA would benefit from stable orbital dynamics, comprehensive coverage of the cislunar domain, and near-zero phase angles that maximize detection SNR. This work presents a trade study addressing the faint-object detection problem and demonstrates the unique advantages of this architecture for cislunar SSA.

2.2 Detection Algorithms

There are a number of methods for detecting faint moving RSOs. Suthakar et al. [19] presents an overview of several object detection schemes suited for SSA covering both traditional methods and deep learning techniques. Some of the more documented standard methods include adjacent frame differencing (AFD), median frame differencing (MFD), and proximity filtering and tracking (PFT), in addition to streak detection methods. Their results highlight that when tasked with detecting faint and prominent RSOs, those algorithms filtered out many of the faint objects. As is shown in section 3.1, the apparent magnitudes of the target RSOs as seen from SEL1 are very faint, so alternative methods are needed to make positive detections from SEL1.

Synthetic tracking or track-before-detect (TBD) methods present a strategy for detecting very faint moving objects. Work by Zhai et al. [23] presents the detection of a 23 apparent magnitude near-Earth asteroid using this technique. Synthetic tracking shifts and adds successive images of a moving target along an unknown velocity vector to increase the SNR of a detection without incurring trailing losses. One example of a TBD algorithm is Integer Pixel Shift and Add (IPSA) [23]. This is a very computationally expensive process because it checks every object velocity hypothesis. The fast discrete X-ray transform (FaXT) [14] is another formulation of a synthetic tracking method. FaXT reduces the computational complexity from $\mathcal{O}(N^5)$ to $\mathcal{O}(N^4)$ by creating and checking short-term tracks. IPSA excels in cases where the searches are targeted and contain some prior knowledge of the velocity hypotheses, or where the number of frames to process is small. FaXT, while introducing some losses compared to IPSA, provides much faster results for uncued faint object detection [13]. Processing data onboard the spacecraft is ideal to reduce required communications

Copyright © 2026 Advanced Maui Optical and Space Surveillance Technologies Conference (AMOS) – www.amostech.com

bandwidth and latency, so the reduced computational complexity of FaXT makes it the preferable algorithm for this mission concept. The speedups associated with this technique are vital given the extremely large search volume of cislunar space.

3. APPROACH AND METHODS

3.1 Characteristic RSO Analysis

In this work, the characteristic RSO is modeled as a lambertian sphere with an albedo of 0.2 and a radius of one meter, approximately the size of a GPS spacecraft [3]. There are more realistic RSO phase functions that exist in literature, but we assume a simple diffuse sphere as a first-order approximation. Using the lambertian sphere model, received irradiance at the sensor E is defined in Eq. 1 in terms of the object's radius R, albedo ρ, distance to sensor d, phase angle α, and the solar irradiance at 1 AU E_0. Eq. 2 relates the received irradiance at the sensor to the apparent magnitude m of the RSO and the zero-point irradiance (E_{zp}). Note that smaller magnitudes correlate to brighter objects. A spacecraft at SEL1 observing cislunar space achieves a near-zero phase angle viewing geometry. This reduces the phase function to unity, simplifying Eq. 1 to Eq. 3.

$$E = E_0 R^2 \left(\frac{2}{3}\rho\right)\left(\frac{\sin(\alpha)+(\pi-\alpha)\cos(\alpha)}{\pi}\right)\left(\frac{1}{d^2}\right) \tag{1}$$

$$m = -2.5\log\left(\frac{E}{E_{zp}}\right) \tag{2}$$

$$E = E_0 R^2 \left(\frac{2}{3}\rho\right)\left(\frac{1}{d^2}\right) \tag{3}$$

3.2 Sensitivity Analysis

Detection characteristics for optical systems are quantified by the signal-to-noise ratio (SNR) calculation shown in Eq. 4. This SNR metric is the ratio of the total received signal to the noise associated with the collection of that data during an integration time t. Noise sources considered here are the detector read noise σ_{read}, detector dark current $n_{dark}t$, background noise $n_{bgd}t$, and signal shot noise $n_{sig}t$, all in e^-/px. The limiting magnitude of an observatory, or the visual magnitude of an object that it can detect with a user-specified SNR and integration time, is defined in Eqns. 5 and 6, where the reference magnitude (m_{ref}) and flux (n_{ref}) are properties of the detector.

$$\text{SNR} = \frac{n_{sig}t}{\sqrt{\sigma_{read}^2 + (n_{sig}+n_{bgd}+n_{dark})t}} \tag{4}$$

$$n_{sig} = \frac{\text{SNR}^2 + \text{SNR}\sqrt{\text{SNR}^2 + 4((n_{bgd}+n_{dark})t + \sigma_{read}^2}}{2t} \tag{5}$$

$$m_{lim} = m_{ref} - 2.5\log\left(\frac{n_{sig}}{n_{ref}}\right) \tag{6}$$

While the integration time can be arbitrarily high for stationary targets, there is an upper limit on integration time for moving targets to avoid streaking. If the target is moving across the detector plane, after some amount of time, its signal received on the detector will move between pixels, which can lead to loss of sensitivity, referred to as trailing loss. To avoid this, the maximum integration time for a given object, or the dwell time τ, is driven by how long it takes the object to cover the angular distance of a pixel. Modeling an observatory with focal length f, aperture diameter D, and pixel size p, the field of view for a particular pixel in the detector (θ_{iFOV}) is given in Eq. 7. An object at distance d from the detector with velocity v tangent to the detector plane has a dwell time τ given by Eq. 8.

$$\theta_{iFOV} \approx \frac{p}{f} \tag{7}$$

Copyright © 2026 Advanced Maui Optical and Space Surveillance Technologies Conference (AMOS) – www.amostech.com

$$\tau \approx \frac{d\theta_{iFOV}}{v} \tag{8}$$

With τ constrained by the orbital motion of the target, images must be stacked to increase the SNR of the detection. Using multiple frames N_f to make a detection modifies the SNR equation, resulting in Eq. 9. As images are added to the stack, the SNR scales as $\sqrt{N_f}$, allowing magnitudes fainter than the limiting magnitude of a single frame to be detected.

$$\begin{aligned} \text{SNR} &= \frac{N_f(n_{sig}t)}{\sqrt{N_f\sigma_{read}^2 + N_f(n_{sig}+n_{bgd}+n_{dark})t}} \\ &= \sqrt{N_f}\left(\frac{n_{sig}t}{\sqrt{\sigma_{read}^2 + (n_{sig}+n_{bgd}+n_{dark})t}}\right) \end{aligned} \tag{9}$$

Along with SNR, other important detection characteristics are the probability of detection (P_D) and the probability of false alarm (P_{FA}). For a given detection, there are two hypotheses: signal on top of the noise, and the null hypothesis (just noise). The P_{FA} is the probability of declaring a detection given that no target is present, while P_D is the probability of declaring a detection given that a target is present. Eqns. 10-11 show the mathematical expression of P_{FA} and P_D for a detection threshold γ, assuming Gaussian statistics.[1].

$$P_{FA} = 1 - \Phi(\gamma) \tag{10}$$

$$P_D = 1 - \Phi(\gamma - \text{SNR}) \tag{11}$$

In the case of TBD algorithms, it is typical to redefine P_{FA} to consider the number of false positives over the entire data cube [23]. Scaling P_{FA} by the number of hypotheses ensures the calculated rate is for the actual detections made in the entire image stack rather than a single frame. The P_{FA} can be redefined as shown in Eq. 12 where N_x, N_y are the dimensions of the detector plane and N_{vx}, N_{vy} are the dimensions of the TBD velocity search space.

$$P_{FA} = N_x N_y N_{vx} N_{vy}(1 - \Phi(\gamma)) \tag{12}$$

There are several losses that must also be accounted for while using track-before-detect methods. The first of these is loss due to *pixelation*, which is the spatial discretization of the point spread function (PSF) due to the pixel grid. The next is the *path quantization* loss in TBD algorithms. As multiple frames are acquired and stacked, TBD algorithms only shift by integer pixels, and this can lead to losses if the true velocities are at the sub-pixel level. The final loss that must be considered is due to *nonlinearities* in the trajectory. TBD methods such as IPSA and FaXT assume linear motion of the target objects; however, orbital dynamics dictate that the motion of these objects is inherently nonlinear. These losses will degrade the performance of the optical system compared to what is calculated explicitly using Eqns. 1-9 as the size of the data cube grows. These losses will be quantified empirically in section 4.3.

3.3 Reference Mission Concept

The concept of operations for the observatory will be designed to prevent trailing loss for an RSO with the fastest expected apparent motion observed from SEL1. To ensure that background star removal can be performed efficiently, the observatory will be sidereally tracking, as illustrated in Fig. 1. The dwell time, τ, will be set for the apparent velocity of a spacecraft while sidereally tracking.

[1] Φ is the cumulative distribution function of the normal distribution.

Copyright © 2026 Advanced Maui Optical and Space Surveillance Technologies Conference (AMOS) – www.amostech.com

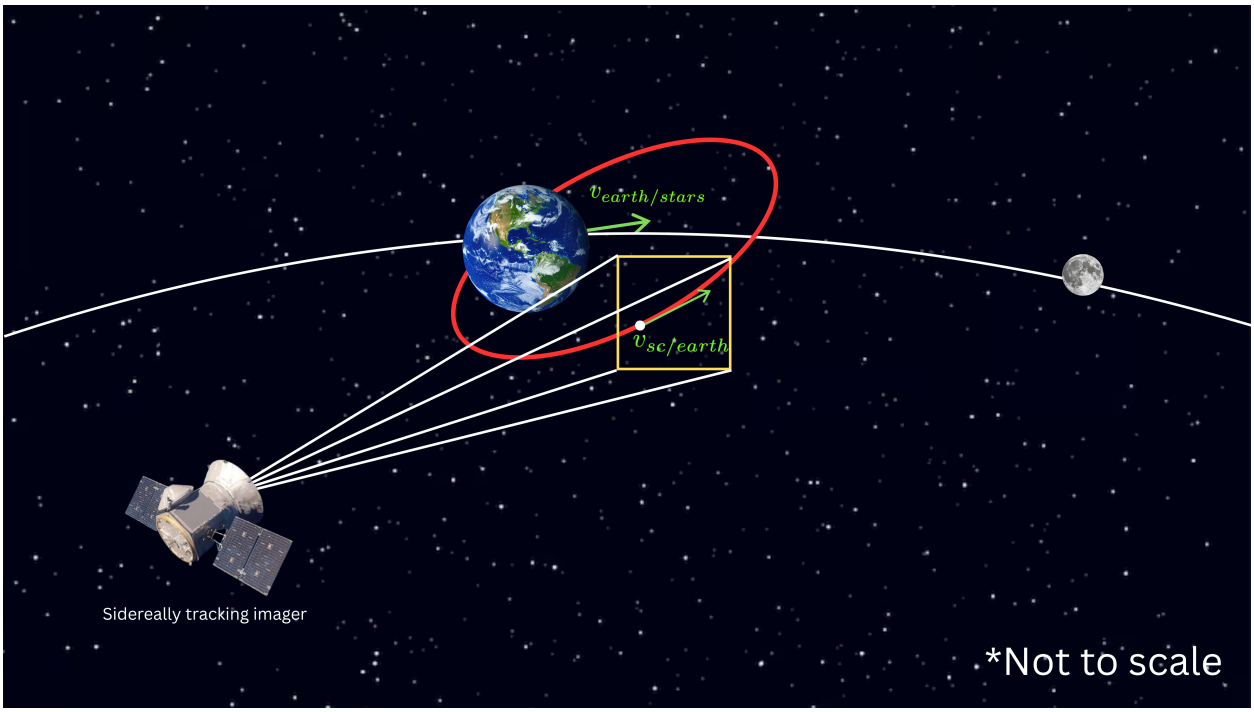


Fig. 1: Mission Concept Diagram. The apparent velocity of the RSO as seen by the sensor is the combination of the orbital velocity of the RSO relative to the Earth and the Earth's motion relative to the stars.

This mission concept centers around the detection of very faint moving objects. For RSOs that are too faint for single-frame detections, TBD algorithms shift and add frames to increase the SNR for a positive detection. This process is computationally expensive, so it is beneficial to look for strategic alternatives to maximize the SNR of a RSO in each frame. One possibility to achieve this is to increase the optical aperture diameter. However, arbitrarily large apertures are not feasible due to large associated costs. An alternative approach to this is to have multiple optical tube assemblies (OTAs) on the same spacecraft that are co-boresighted. This allows for the stacking of identical raw frames to form a single composite frame, with a new SNR scaled as $\sqrt{N_{aper}}$.

Second, if a target RSO were observed while the observatory was tracking the motion of the Earth, a longer integration time could be utilized due to a decrease in apparent relative motion. When the observatory is sidereally tracking, a large portion of the apparent RSO velocity is due to the known motion of the Earth. In the Earth-tracking concept, removal of background stars would not be possible. To satisfy star removal constraints while maximizing dwell time, we developed a hybrid approach. We synthetically track the known motion of the Earth, which allows for a longer effective dwell time (τ_{eff}) and provides a higher single-frame SNR. This process is the same as a track-before-detect algorithm, except the velocity of the object is known, so no blind searches are required. Synthetically tracking the Earth creates co-added frames with this effective dwell time, while the observatory is tracking sidereally during imaging. Fig. 2 shows the benefit that can be gained with this hybrid approach. After star subtraction, shifting along the motion of the Earth reduces the apparent motion of the target, which increases the effective integration time. With the reduced motion of the target RSO, more signal can be captured before the target moves out of one pixel in the Earth-tracking stack, increasing the SNR of frames processed with FaXT.

Copyright © 2026 Advanced Maui Optical and Space Surveillance Technologies Conference (AMOS) – www.amostech.com

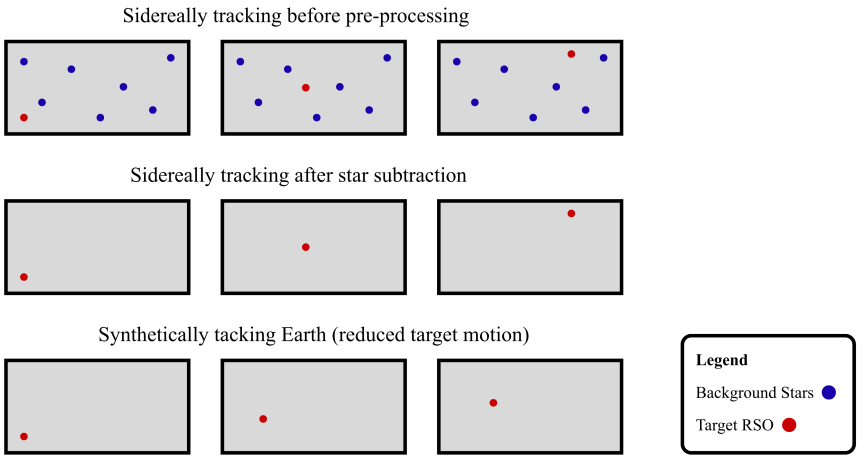


Fig. 2: Graphic showing the difference between sidereally tracking and Earth-tracking. The top row represents the raw captured imagery. Using median subtraction, background stars will be removed from the frame, leaving just the RSO. The bottom row shows the benefit of synthetically tracking the Earth after operating the sensor in sidereal tracking mode, resulting in reduced target motion between successive frames.

The proposed stacking concept is outlined in Fig. 3. The identical frames from the co-boresighted OTAs are stacked, and stars are removed, after which these composite frames are synthetically tracked along the Earth's known motion. These stacks with the target RSOs in different locations will now form one stack with the RSO within a single pixel. A number of these stacks will then be processed with TBD methods allowing for un-cued detections to be made of RSOs.

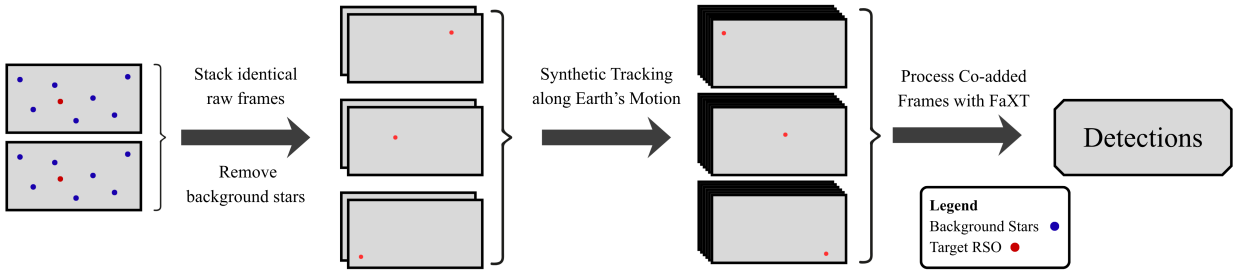


Fig. 3: SEL1 SSA Observer stacking procedure. Identical raw frames have their background stars removed and are added into composite frames. Composite frames are added together along the known velocity of the Earth to reduce the target motion from several pixels into a single pixel. These newly formed co-added frames are processed with FaXT to make a detection.

An additional consideration is the relationship between the number of co-added frames and the number of OTAs on the spacecraft. In the theoretical limit, SNR scales as $\sqrt{N_f}$ with the number of frames, as shown in Eq. 9. Thus, doubling either the number of OTAs or the number of co-added frames produces the same theoretical SNR improvement. In practice, however, the two approaches are not equivalent. Increasing the number of co-added frames increases the total integration time of the stack, causing the RSO trajectory to exhibit greater nonlinearity and consequently incur larger processing losses. Additionally, increasing the number of frames increases the revisit time required to scan a given search volume.

3.4 Payload Trade Study

The approach to this study starts with defining requirements and constraints for the observatory focused on target RSO orbits and photometry, as well as the capabilities of the optical payload. Once outlined, potential configurations of the optical payload are analyzed for their ability to detect the characteristic RSO. COTS availability is required to limit

Copyright © 2026 Advanced Maui Optical and Space Surveillance Technologies Conference (AMOS) – www.amostech.com

cost. The optical parameters under consideration for this design study are outlined in Table 1 based on preliminary analyses and the COTS availability consideration.

Table 1: Payload Trade Study Parameters

Parameter	**Limits**
Aperture size, D (meters)	0.1-0.5
Focal Ratio, $f/\#$	$1-3$
Number of Apertures, N_{aper}	≤ 4

The specific choice of detector and the size of its pixels are explicitly intertwined with the performance of the observatory. For this analysis, a well-documented sensor is chosen as a baseline, and its parameters are kept constant. This does not imply a final design choice, but rather just a baseline of performance. Many trade parameters for this design are driven by upstream requirements, and Fig. 4 shows the interconnected nature of the analysis.

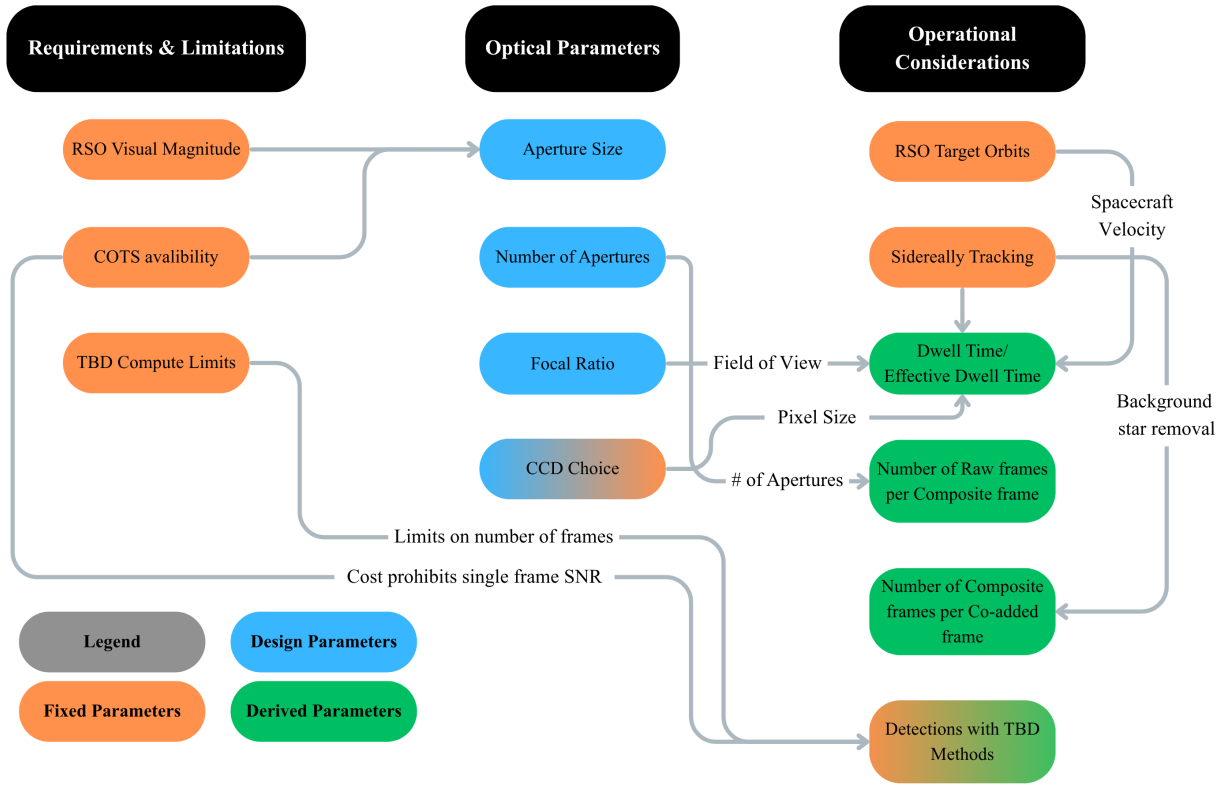


Fig. 4: Flowchart outlining the fixed, design, and derived parameters of the trade study.[2] Many components of the design are derived from either requirements or practical limitations. Arrows denote flows in logic or physics, and text explains the relationship.

Driving requirements for the observatory include properties of the characteristic RSO and the COTS availability of the optical system. Detection of faint RSOs motivates larger aperture diameters, whereas the COTS availability limits the maximum size available. The focal ratio informs how "fast" the optics are, and thus what integration time is required

[2]CCD Choice is listed both as a fixed and design parameter. This is defined in this manner because while the CCD is fixed for this feasibility analysis, it would be a design parameter in future work.

Copyright © 2026 Advanced Maui Optical and Space Surveillance Technologies Conference (AMOS) – www.amostech.com

to detect the object, impacting both the dwell time and single-frame SNR of an object. Operationally speaking, aspects such as the characteristic RSO orbit and the decision to sidereally track to allow for background subtraction drive the relationship between τ and τ_{eff}. This directly informs how many each of raw, composite, and co-added frames exist for the specific architecture.

4. RESULTS

4.1 Reference Scenario

Representative Target Orbits To support the performance analysis, we first define a set of representative orbits to serve as reference targets. Orbits are selected to cover medium Earth orbits (MEO) and above. Low Earth orbits (LEO) are not considered due to proximity to the Earth's limb and detection availability from traditional SSA systems. Table 2 and Fig. 5 show example orbits and their associated arcsec/s velocities that are relevant to cislunar SSA. These orbits were identified due to their use in current and planned cislunar operations. The trajectories from the associated missions are found in the JPL Horizons database [10].

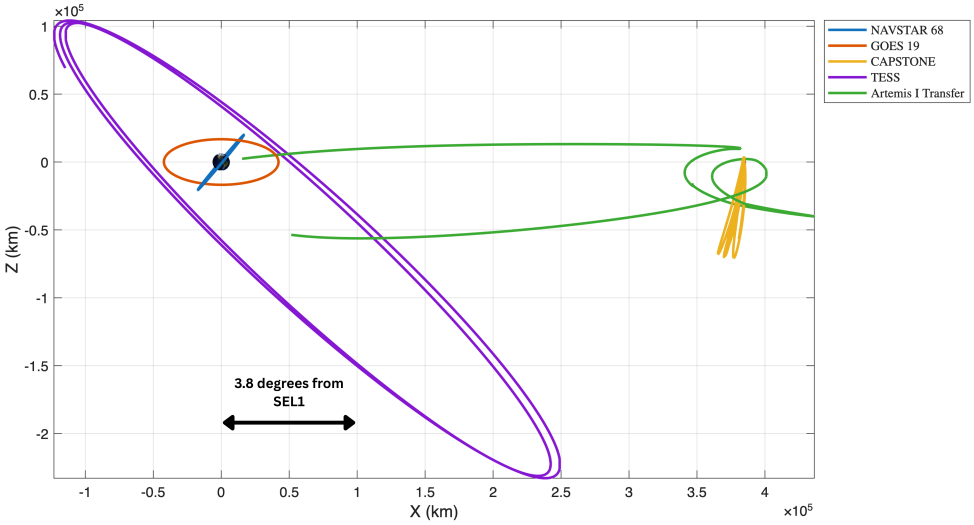


Fig. 5: Select orbits in cislunar space as viewed from SEL1 [10][3].

Table 2: Orbits and angular velocities for considered trajectories. 99^{th} percentile used for each trajectory [10]

Orbital Regime	Angular Velocity (Sidereal)	Angular Velocity (Earth Tracking)
MEO (NAVSTAR 68) [4]	3.4"/s	0.4"/s
GEO (GOES 19) [8]	3.4"/s	0.3"/s
Lunar-Resonant (TESS) [21]	3.3"/s	0.2"/s
Lunar Transfer (ARTEMIS I) [1]	3.4"/s	0.4"/s
NRHO (CAPSTONE) [7]	3.3"/s	0.3"/s

The analyzed MEO trajectory has the largest apparent velocity on the detector plane, and appears most nonlinear on average due to its small orbital radius. In these calculations, the 22nd apparent magnitude RSO is assumed for each case, and listed missions/spacecraft only provide the reference trajectories.

Detector Properties For a baseline detector, we selected the MIT/LL CCID-80, which is the sensor onboard the TESS spacecraft [21]. The detector was chosen as a baseline option due to its well-documented optical properties and

[3]Lunar transfer and NRHO orbits are plotted in a rotating frame for visual clarity.

Copyright © 2026 Advanced Maui Optical and Space Surveillance Technologies Conference (AMOS) – www.amostech.com

noise sources, which are given in Table 3, as well as similarities in the size of the TESS 10.5 cm OTAs to our own trade space [21].

Table 3: MIT/LL CCID-80 Specs [21]

Property	**Value**
CCD Dimensions	2048 x 2048 pixels in imaging array
Pixel Size	15 μm
Pixel Depth	100 μm
σ_{read}	7-11 e^-/s
n_{dark}	negligible
Quantum Efficiency	0.9

Detection Statistics We are also assuming a sky background of 22.2 visual magnitude per arcsec^2 for this study, calculated empirically from TESS pixel files and calibration data [20]. For this feasibility study, we will be imposing a P_{FA} of 1% and P_D of 50%, resulting in a SNR requirement of 7.5 to meet these constraints.

4.2 Performance Upper Bound

This section outlines the upper bound on performance of the baseline cislunar SSA observatory design excluding losses due to pixelation, path quantization, and nonlinearity. The following sections will expand upon the losses discussed in section 3.2, and outline how those losses impact design choices. Through the development of an observatory simulation tool, we modeled the performance of the SEL1 SSA spacecraft's ability to detect the characteristic RSO with a varying quantity of OTAs, aperture diameters, and focal ratios in order to come up with a feasible set of potential designs. These results will be used to inform design decisions and trades for a candidate design if it were to be developed to completion.

Parameters that are varied in this trade study to create the feasible set of designs are: observatory aperture size, observatory focal ratio, number of OTAs, and number of frames processed with FaXT. As mentioned in section 3.3, doubling the number of apertures and doubling the number of frames processed by a TBD algorithm has the same effect on the SNR of the detection. For simplicity, we define a new quantity, the number of effective frames (N_{eff}), as defined in Eq. 13. This results in the last two design parameters collapsing into a single design trade, the number of effective frames. Note that due to algorithmic requirements, N_{FaXT} must be stacks of 2^x frames [14]. The maximum N_{FaXT} and $N_{apertures}$ that we consider are 256 and 4, respectively.

$$N_{eff} = N_{apertures} \times N_{FaXT} \tag{13}$$

Fig. 6 shows the SNR achieved by the SEL1 SSA observatory when detecting the characteristic RSO in MEO, identified as the most demanding case. Combinations of aperture diameter, focal ratio, and N_{eff} that achieve an SNR above the desired threshold represent feasible designs under the current assumptions regarding losses. For the 22nd-magnitude RSO and the requirement of $P_{FA} = 1\%$ and $P_D = 50\%$, the required SNR is 7.5, represented by the orange dashed line. Fig. 6 informs the reader of the set of feasible designs given a requirement on SNR.

Copyright © 2026 Advanced Maui Optical and Space Surveillance Technologies Conference (AMOS) – www.amostech.com

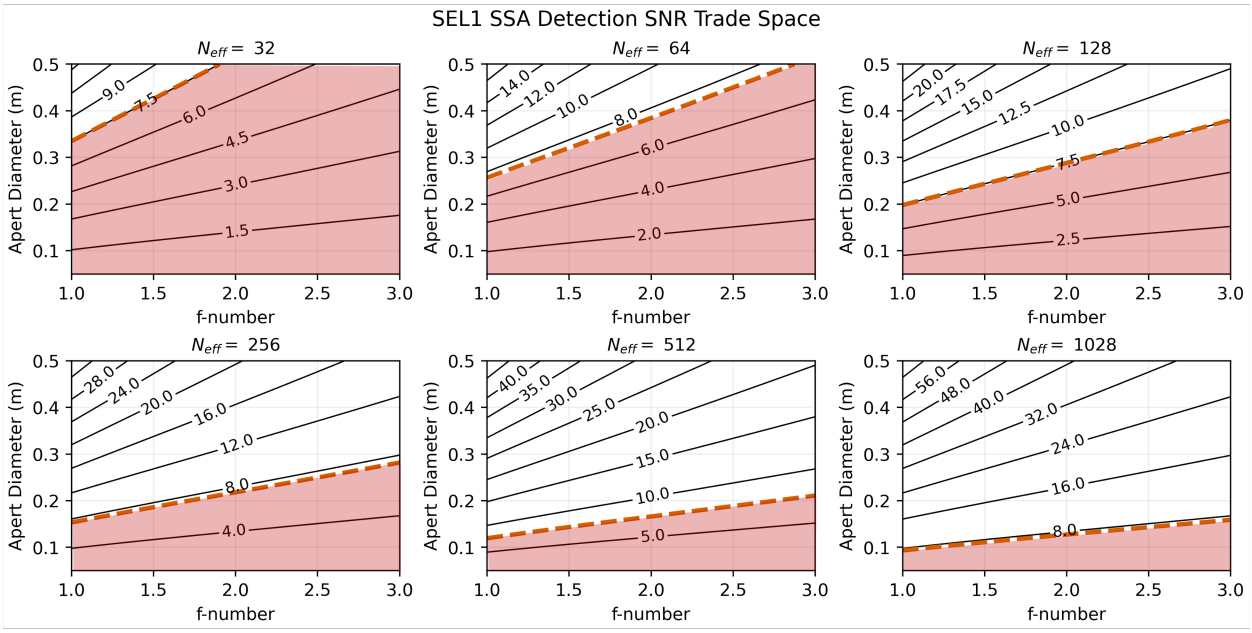


Fig. 6: SNR of the characteristic RSO as seen from the SEL1 cislunar SSA observatory under no losses due to pixelation, path quantization, or nonlinear motion. The orange line denotes the 7.5 SNR threshold required to achieve the 1% P_{FA} and 50% P_D that are required. Designs in the red area do not meet requirements. Each plot is shown for a number of effective frames, representing the product of the frames processed with FaXT and the number of OTAs. Anything above the orange line is a feasible design in the ideal case.

Once feasible design parameters are identified for a specific SNR requirement, there are trade-offs that may favor one design over another, such as increased cost. A detail that this analysis abstracts out is the nuance between changing $N_{apertures}$ and N_{FaXT}. The threshold SNR of 7.5 that is highlighted in Fig. 6 in the subplot for N_{eff} = 256 can be achieved with all of the combinations provided in Table 4.

Table 4: Examples of how effective frames can be broken up into $N_{apertures}$ and N_{FaXT}

Number of Apertures	**Frames processed with FaXT**
$N_{aper} = 1$	$N_{FaXT} = 256$
$N_{aper} = 2$	$N_{FaXT} = 128$
$N_{aper} = 4$	$N_{FaXT} = 64$

Each architecture presents distinct advantages and disadvantages. More apertures add expense and complexity to the optical design, whereas an increased number of frames results in more processing time for FaXT, more losses due to nonlinearity (covered in section 4.3), and longer revisit times.

Another dimension of the problem is the tradeoff between aperture size and N_{eff}. Increasing both of these parameters will offer the user increased SNRs of detection. Fig. 7 explores this trade for an OTA with a focal ratio of f/1.4. Under the RSO and detection statistics assumed in this study, the SNR 7.5 contour shown in orange defines the Pareto front. The designer must weigh the higher cost of larger optics against the increased losses associated with more effective frames. The knee in the curve near 150 effective frames has significant design implications, as moving to either side requires a rapid increase in one parameter for relatively little improvement in the other.

Copyright © 2026 Advanced Maui Optical and Space Surveillance Technologies Conference (AMOS) – www.amostech.com

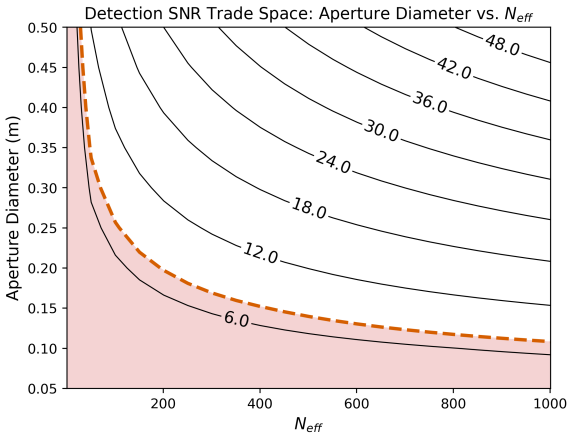


Fig. 7: SNR as a function of aperture diameter and N_{eff}. The orange line is the SNR 7.5 threshold. Any designs in the red shaded area do not meet requirements. The number of required effective frames increases gradually as the aperture is reduced from 0.5 m at first before it grows rapidly as the diameter approaches 0.1 m.

4.3 Signal Loss with Image Processing

The sensitivity losses considered in this analysis include pixelation, path quantization loss, and losses due to nonlinear motion of the RSOs on the detector plane. Pixelation and path quantization loss of FaXT have been characterized to be 30% to 40% depending on specifics of the frames for linear trajectories [13]. The effect of non-linearity is unique to different mission scenarios and can be assessed by simulating non-linear object motion on the detector plane and analyzing the SNRs after stacking with FaXT. Although dwell times are selected to minimize trailing losses, some residual losses are unavoidable and are neglected in this study.

This section presents simulations characterizing the impact of losses on detection SNR for the characteristic RSO. Simulated imagery for the characteristic RSO on the orbit with the largest accelerations (MEO) was processed for a sweep of per-frame accelerations that would be expected[4] for optical designs within the parameters of the trade study. Target position on the focal plane array during the detection period is modeled as second order equations as shown in Eqns. 14-15.

$$x = a_x n^2 + b_x n + c_x \tag{14}$$

$$y = a_y n^2 + b_y n + c_y \tag{15}$$

The actual motion of the RSO was projected onto the detector plane, where it was parametrized with Eqns. 14-15. Images were then simulated with a target undergoing motion according to that parametrization, identical in both x and y to force an extreme case. FaXT was run on the stacks, where the SNR of the detection was reported and compared to the theoretical SNR given by Eq. 9. Fig. 8 shows the percentage of the theoretical SNR retained after stacking 256 frames with FaXT. The vertical lines represent reference designs with accelerations corresponding to the parameterization of the projected motion of a MEO RSO on the detector plane. The results shown are averaged over a velocity sweep from zero initial velocity to the initial velocity where the largest velocity in the data cube does not exceed one pixel per frame[5]. Results of this simulation show that losses between 30% and 80% are expected when processing 256 frames in FaXT. The reported acceleration values are those of the parametrization in each direction, not of the actual object motion.

[4]While the RSO's acceleration is deterministic from its astrodynamic state, the parametrization of its apparent motion on the focal plane array depends on quantities such as field of view and dwell time.

[5]This sweep covers all expected velocities and accelerations of the RSOs.

Copyright © 2026 Advanced Maui Optical and Space Surveillance Technologies Conference (AMOS) – www.amostech.com

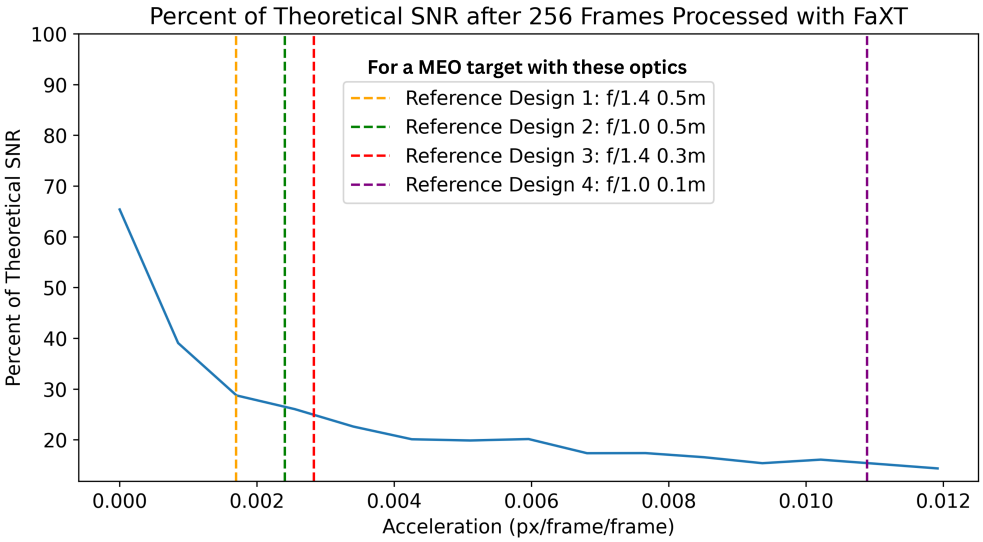


Fig. 8: Percentage of the theoretical SNR after processing 256 frames with FaXT. Results are an averaged velocity sweep from zero initial velocity to the initial velocity for which the maximum velocity in the data cube does not exceed one pixel per frame. Dashed lines represent acceleration projections on the detector plane for select reference optical designs. Expected losses range from 30% to 80%.

Extreme losses of up to 80% corresponding to certain design architectures further refine the set of feasible solutions presented in section 4.2. To detect the same object, choosing an architecture that results in a longer τ_{eff} for the same pre-FaXT SNRs comes at the expense of increased losses. When more frames are used, that amounts to larger integration times, which in turn results in the motion of the RSO on the detector appearing more nonlinear. Table 5 shows the reference designs, their values for τ_{eff} and the associated losses.

Table 5: Effective dwell times and SNR % losses for the reference designs

Reference #	Focal Ratio	Aperture Diameter (m)	τ_{eff} (sec)	Loss from FaXT
1	f/1.4	0.5	8.2	72%
2	f/1.0	0.5	11.5	74%
3	f/1.4	0.3	13.6	76%
4	f/1.0	0.1	57.3	85%

In the most demanding cases, such as reference design four, image-processing losses exceed 80%, while reference design one, with the shortest τ_{eff}, incurs a 72% loss. Selecting an architecture that requires 256 frames to be processed with FaXT can have significant implications for the resulting SNR losses. In contrast, limiting FaXT processing to 64 frames substantially reduces these losses. Fig. 9 shows the percentage of theoretical SNR retained for the same scenario as Fig. 8, but for 64 frames processed with FaXT where the losses range from 30% to 60%. This represents a major design choice when developing this architecture. It favors configurations that result in lower effective dwell times and smaller numbers of frames processed with FaXT. Optimal design choices in terms of detection capabilities will center around larger apertures and more OTAs on the payload.

Copyright © 2026 Advanced Maui Optical and Space Surveillance Technologies Conference (AMOS) – www.amostech.com

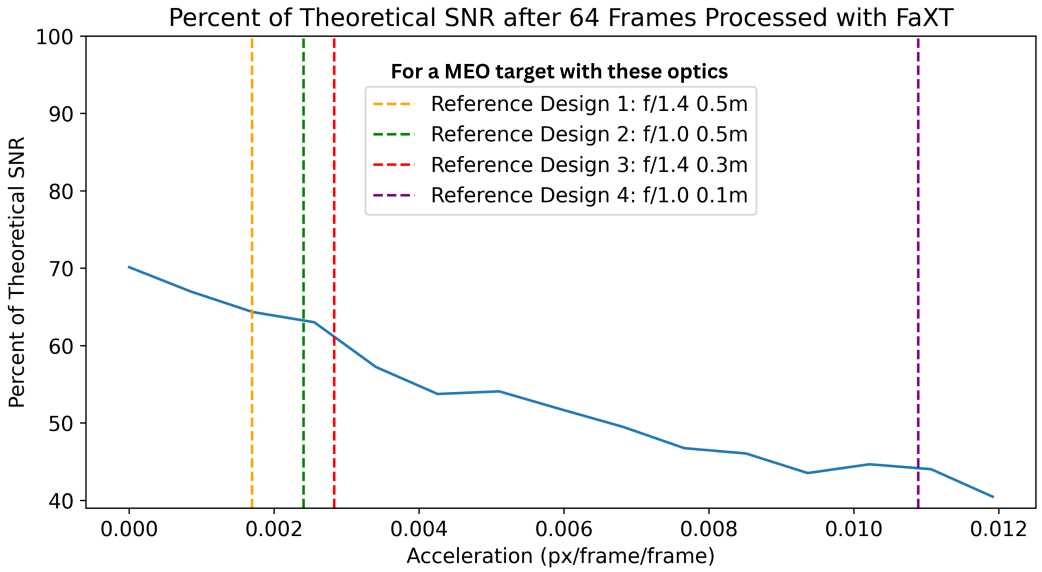


Fig. 9: Percentage of the theoretical SNR after processing 64 frames with FaXT. Results are an averaged velocity sweep from zero initial velocity to the initial velocity for which the maximum velocity in the data cube does not exceed one pixel per frame. Dashed lines represent acceleration projections on the detector plane for select reference optical designs. Expected losses range from 30% to 60%.

As mentioned in section 3.3, in the ideal case, doubling the number of frames processed with FaXT and the number of apertures has the same effect. However, when losses are considered, this assumption breaks down. Fig. 10 shows this nuance for optical reference design three. When examining different breakdowns of the effective frames, the four-OTA design that processes 32 frames with FaXT only incurs a 13% loss, whereas the single OTA design incurs a 64% loss with 128 FaXT frames. Having more OTAs and fewer frames leads to decreased losses at the expense of increased optical complexity.

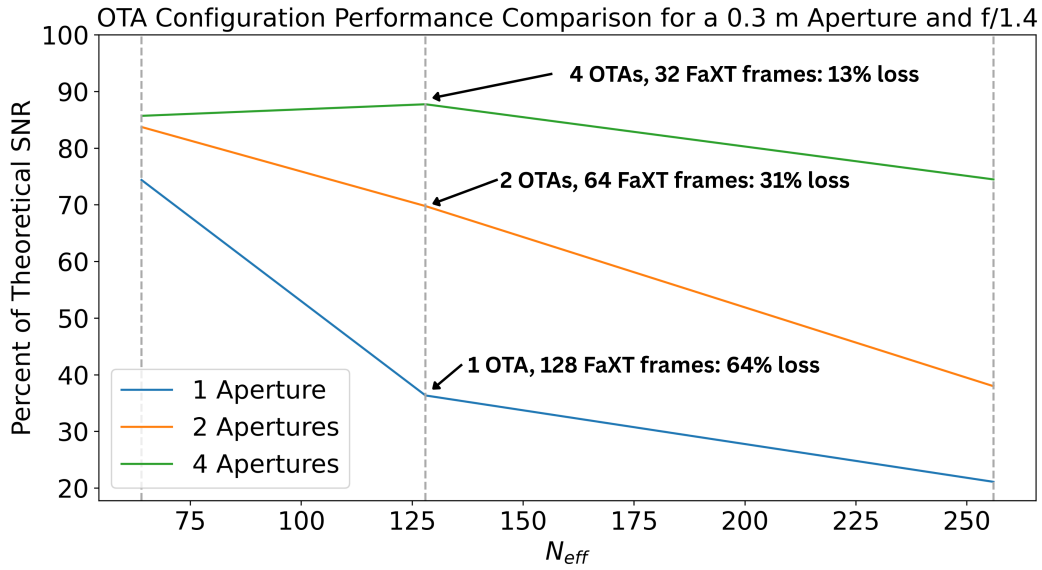


Fig. 10: Performance of 0.3 m f/1.4 optics across OTA configurations for a sweep of effective frames. The four-aperture design incurs fewer losses for the same effective frames due to the decrease in N_{FaXT} associated with that design.

Copyright © 2026 Advanced Maui Optical and Space Surveillance Technologies Conference (AMOS) – www.amostech.com

The results presented in this section represent the most demanding acceleration cases considered for the fastest-moving objects (MEO). The losses shown in Figs. 8-10 therefore represent an extreme case and provide a conservative lower bound on system performance. Further analysis could evaluate nominal detection scenarios and quantify the losses associated with less demanding RSO dynamics.

4.4 Sample Design

This section will outline the optical properties and stacking procedure for reference design three from Table 5. This is not an optimized design, but rather a solidified example to show the feasibility of the concept. The reference observatory design properties are given in Table 6. Given the design parameters, the optical parameters can be calculated using the equations defined in section 3, which are given in Table 7.

Table 6: Reference Observatory Design Parameters

Parameter	**Value**
Aperture Diameter	0.3 meters
Focal Ratio	f/1.4
Number of OTAs	4
Detector	MIT/LL CCID-80

Table 7: Reference Observatory Optical Parameters

Parameter	**Value**
τ	1.608 seconds
τ_{eff}	13.647 seconds
θ_{iFOV}	35.7 μrad
Sample Distance	53.571 km
Composite frames per Co-added frame	9 frames

From these parameters, the stacking procedure can be defined. Each of the four OTAs produces a single raw frame, which are then stacked to form a single composite frame. Based on the ratio of τ_{eff} to τ, nine composite frames are synthetically tracked along the Earth's motion to form one co-added frame. Thus, each frame that is passed to FaXT for analysis consists of one co-added frame, corresponding to 9 composite frames, or 36 raw frames.

As established in section 4.1, the characteristic RSO has a magnitude of 22, and an SNR of 7.5 is required to achieve a P_{FA} of 1% and a P_D of 50%. The final performance results for this example design are presented in Table 8. While these results do not represent an optimal design, they represent a feasible design that motivates further investigation into optimization of this mission concept.

Table 8: Reference Observatory Design Performance

Parameter	**Value**
Theoretical SNR	14.5
Total Raw frames	2304 frames
Total Composite frames	576 frames
N_{FaXT} (Total Co-added frames)	64 frames
N_{eff}	256 frames
SNR per co-added frame	1.82
SNR after FaXT	10.58
% Loss	27.14

This observatory design closes and satisfies all requirements established earlier in the study. It is also worth noting that the number of frames processed by FaXT is sufficiently low that the effects of nonlinearities are negligible, with

Copyright © 2026 Advanced Maui Optical and Space Surveillance Technologies Conference (AMOS) – www.amostech.com

the resulting SNR loss being comparable to that of the linear-motion case [13]. For comparison, a 1-OTA design with the same number of effective frames and the same hypothetical loss characteristics achieves a final SNR of 3.11, corresponding to a substantially larger 78.5% loss. These results align with the simulated data analyzed in Fig. 10 for the 256 effective frames case. Returning to the regions of feasible designs in Fig. 6, where no single architecture is clearly preferred, accounting for image-processing losses favors architectures with more OTAs over those requiring a greater number of FaXT frames in terms of final SNR. This introduces an additional design tradeoff between increased optical complexity from additional OTAs and the greater SNR losses associated with processing more frames with FaXT.

5. CONCLUSION AND FUTURE WORK

In this paper, we present an alternate cislunar SSA architecture centered around an observatory placed at SEL1. This viewing location provides stable orbits for the observatory, a repeatable view of cislunar space, and near-zero phase angles for target illumination. This study shows that the difficulties of detection at extreme distances can be resolved with the use of moderately-sized optical designs when paired with novel track-before-detect algorithms and a refined concept of operations. The example observatory design uses multiple co-boresighted OTAs and synthetic tracking along known motion vectors to increase the SNR of the images before un-cued detections are made utilizing FaXT. An example design for an observatory with four co-boresighted 30 cm f/1.4 OTAs has the potential to detect spacecraft modeled as a meter lambertian sphere at a distance of 1.5 Gm, appearing as 22nd magnitude from SEL1 with a 50% probability of detection and 1% false alarm rate. Having more OTAs can reduce the effect of non-linearity on sensitivity but will incur additional cost. An additional trade study is needed to design a practical operational system that will meet a larger set of requirements.

Future work on this topic includes revisiting several assumptions about sky background models, Earth and Moon exclusion zones, detector choice, and trailing losses to provide a more comprehensive analysis of the observatory detection capabilities. Another performance metric that must be explored further is revisit time. The reference design above with $\tau = 1.608$ seconds and 576 composite frames has a capture time per observation of about 16 min. Further work is required to define a comprehensive cislunar search volume and time between observations required for slew and settling. The total time it takes to scan the desired search space is an important consideration when discussing the feasibility of an SSA architecture.

This work provides a preliminary concept design for a novel SSA concept at SEL1. We presented a systematic approach to designing a payload and concept of operations, unique strategies to improve sensitivity, and provide reference design points accounting for common losses. This work serves as a starting point for future system and mission design for SEL1 cislunar SSA concepts, a compelling addition to existing cislunar SSA architectures.

ACKNOWLEDGMENTS

The authors would like to thank Sophia Matthews for her assistance in investigating the losses under acceleration.

Copyright © 2026 Advanced Maui Optical and Space Surveillance Technologies Conference (AMOS) – www.amostech.com

REFERENCES

[1] Amelia L Batcha, Jacob Williams, Timothy F Dawn, Jeffrey P Gutkowski, Maxon V Widner, Sarah L Smallwood, Brian J Killeen, Elizabeth C Williams, and Robert E Harpold. Artemis I Trajectory Design and Optimization. In *2020 AAS/AIAA Astrodynamics Specialist Conference*, pages 20–649. AAS, 2020.

[2] MEP Chatters and MBJ Crothers. AU-18 Space Primer, ch. Space Surveillance Network, 2009.

[3] eoPortal. Satellite Missions Catalogue: GPS, 2026.

[4] S.C. Fisher and K. Ghassemi. GPS IIF-the Next Generation. *Proceedings of the IEEE*, 87(1):24–47, 1999.

[5] Erin E Fowler, Stella B Hurtt, and Derek A Paley. Orbit Design for Cislunar Space Domain Awareness. In *2nd IAA Conference on Space Situational Awareness (ICSSA), Washington, District of Columbia*, 2020.

[6] Carolin Frueh, Kathleen Howell, Kyle J DeMars, and Surabhi Bhadauria. Cislunar Space Situational Awareness. In *31st AIAA/AAS Space Flight Mechanics Meeting*, volume 144, 2021.

[7] Thomas Gardner, Brad Cheetham, Alec Forsman, Cameron Meek, Ethan Kayser, Jeff Parker, Michael Thompson, Tristan Latchu, Rebecca Rogers, Brennan Bryant, et al. Capstone: A Cubesat Pathfinder for the Lunar Gateway Ecosystem. 2021.

[8] Steven J. Goodman. Chapter 1 - GOES-R Series Introduction. In Steven J. Goodman, Timothy J. Schmit, Jaime Daniels, and Robert J. Redmon, editors, *The GOES-R Series*, pages 1–3. Elsevier, 2020.

[9] Marcus J Holzinger, C Channing Chow, and Peter Garretson. A Primer on Cislunar Space. 2021.

[10] Jet Propulsion Laboratory, Solar System Dynamics Group. JPL Horizons On-Line Ephemeris System, 2026.

[11] Thomas Joyce, Ryland Phipps, Craig Jacobson, Tanner Campbell, Adam Battle, Daniel Estévez, Roberto Furfaro, and Vishnu Reddy. Passive RF Observations for Cislunar Objects. In *Proceedings of the Advanced Maui Optical and Space Surveillance (AMOS) Technologies Conference*, page 121, 2023.

[12] Air Force Research Laboratory. Oracle Family of Systems, 2026.

[13] Sophia Matthews and Tam Nguyen. Performance Assessment of Track-Before-Detect Algorithms and Post-Search Refinement Methods. Submitted, 2026.

[14] Tam Nguyen, Deborah F. Woods, Jessica Ruprecht, and Jonathan Birge. Efficient Search and Detection of Faint Moving Objects in Image Data. *The Astronomical Journal*, 167(3):113, March 2024.

[15] Craig Roberts, Sara Case, John Reagoso, and Cassandra Webster. Early Mission Maneuver Operations for the Deep Space Climate Observatory Sun-Earth L1 Libration Point Mission. In *AIAA/AAS Astrodynamics Specialist Conference*, number GSFC-E-DAA-TN25055, 2015.

[16] Craig Roberts, Sarah Case, and John Reagoso. LISSAJOUS Orbit Control for the Deep Space Climate Observatory Sun-Earth L1 Libration Point Mission. In *AIAA/AAS Astrodynamics Specialist Conference*, number AAS 15-611, 2015.

[17] Craig E Roberts. Long Term Missions at the Sun-Earth Libration Point L1: ACE, SOHO, AND WIND. In *AAS/AIAA Astrodynamics Specialist Conference*, number GSFC. CP. 4786.2011, 2011.

[18] Clint Spesard and Robert A. Bettinger. Preliminary Lunar Surface SSA Architecture Optimization for the Observabilty of Cislunar and Lunar Resident Space Objects. In *AIAA SCITECH 2024 Forum*, Orlando, FL, January 2024. American Institute of Aeronautics and Astronautics.

[19] Vithurshan Suthakar, Aiden Alexander Sanvido, Randa Qashoa, and Regina S. K. Lee. Comparative Analysis of Resident Space Object (RSO) Detection Methods. *Sensors*, 23(24):9668, December 2023.

[20] TESS Team. TESS Pixel Files: All Sectors, 2022.

[21] Roland Vanderspek et al. *TESS Instrument Handbook*. MIT Kavli Institute, 2018.

[22] Jacob K. Vendl and Marcus J. Holzinger. Cislunar Periodic Orbit Analysis for Persistent Space Object Detection Capability. *Journal of Spacecraft and Rockets*, 58(4):1174–1185, July 2021.

[23] Chengxing Zhai, Michael Shao, Bijan Nemati, Thomas Werne, Hanying Zhou, Slava G. Turyshev, Jagmit Sandhu, Gregg Hallinan, and Leon K. Harding. Detection of a Faint Fast-Moving Near-Earth Asteroid using the Synthetic Tracking Technique. *The Astrophysical Journal*, 792(1):60, August 2014.

[24] Peter Zimmer, John T McGraw, and Mark R Ackermann. Cislunar SSA/SDA from the Lunar Surface: COTS Imagers on Commercial Landers. In *Advanced Maui Optical and Space Surveillance Technologies (AMOS) Conference*, pages 14–17. Curran Assoc., Inc. Redhook, NY, 2021.

Copyright © 2026 Advanced Maui Optical and Space Surveillance Technologies Conference (AMOS) – www.amostech.com